Atmos. Chem. Phys. Discuss., https://doi.org/10.5194/acp-2017-1000
Manuscript under review for journal Atmos. Chem. Phys.
Discussion started: 14 December 2017


# Comparison of the optical properties of pure and transported anthropogenic dusts measured by ground-based Lidar

Zhijuan Zhang[1], Bin Chen[1,*], Jianping Huang[1], Jingjing Liu[2], Jianrong Bi[1], Tian Zhou[1], Zhongwei Huang[1]

[1]Key Laboratory for Semi-Arid Climate Change of the Ministry of Education, College of Atmospheric Sciences, Lanzhou University, Lanzhou, 730000, China
[2]School of Mechanical and Instrument Engineering, Xi’an University of Technology, Xi’an 710048, China

[*]Corresponding author：chenbin@lzu.edu.cn

Atmos. Chem. Phys. Discuss., https://doi.org/10.5194/acp-2017-1000
Manuscript under review for journal Atmos. Chem. Phys.
Discussion started: 14 December 2017


**Abstract**

In this study, the optical properties of pure dust (PDU) and transported anthropogenic dust (TDU) (also defined as polluted dust) are compared by using ground-based Lidar data for the period from October 2009 to June 2013. The total attenuated backscattering coefficient at 532 nm, the linear volume depolarization ratio and the color ratio are derived from the L2S-SM-II dual-band polarization Lidar. We found that the TDU has a spherical shape, a small linear volume depolarization ratio and a large color ratio which representing its large particle sizes. The threshold value delineating PDU and TDU was approximately 0.2, which is the same as the threshold value used in the CALIPSO CAD algorithm. The histogram of the attenuated backscattering coefficients and the color ratios of pure dust shows two peaks, but that for the transported anthropogenic dust shows no significant peak and a nearly uniform distribution. The ground-based Lidar results confirm that both the transported anthropogenic dust and pure dust can be detected by air-borne or ground-based Lidar measurements.

## 1 Introduction

Dust aerosols are one of the most important aerosol types in the troposphere and are an important source of atmospheric aerosols (Huang et al., 2014). Dust can impact the earth-atmosphere radiation budget by absorbing and scattering solar radiation as well as by emitting IR radiation (direct effect) (e.g., Sokolik and Toon, 1996; Li, 2004; Shi et al., 2005, Huang et al., 2009), altering the optical properties and lifetimes of clouds (indirect effect) (e.g., Sassen, 2002), increasing the evaporation of cloud droplets and further reducing the CWP (Cloud Water Path) by the means of warming clouds (semi-direct effect) (Huang et al., 2006b), all of which can eventually change the climate (Luo et al., 2000, Twomey et al., 1984; Huang et al., 2005, 2006a, 2006b;), especially in semi-arid regions in East Asia (Huang et al., 2010, 2014). Dust aerosols, or mineral dusts, have obvious heating or cooling effects that can change the atmospheric thermal circulations and dynamic conditions, making dust aerosols one of the important factors triggering global environmental problems. However, the existing atmospheric dust load cannot be explained by natural sources alone. The atmospheric dust load that originates from soils disturbed by human activities, such as land use practices, can be interpreted as "anthropogenic" dusts (Tegen and Fung, 1995). Anthropogenic dusts are those produced by human activities on disturbed soils, which are found mainly in croplands, pasturelands, and urbanized regions, and are a subset of the total dust load, which includes natural sources from desert regions (Huang et al., 2015).

Local anthropogenic dust aerosols associated with human activities, such as agricultural and industrial activities, accounted for 25% of the total dust burden in the atmosphere (Huang et al., 2015). These anthropogenic dusts can increase dust loading, which, in turn, affects radiative forcing (Tegen and Fung, 1995). Huang et al. (2015) found that local anthropogenic dust aerosols from human activities, such as agriculture, industrial activity, transportation, and overgrazing, account for approximately 25% of the global continental dust load. Of these anthropogenic dust aerosols, more than 53% come from semi-arid and semi-wet regions (Guan et al., 2016). The annual mean anthropogenic dust column burden values range from a 0.42 g $m^{-2}$ maximum in India to a 0.12 g $m^{-2}$ minimum in North America. Previous works have also explored the global relationship between anthropogenic dusts and population over semi-arid regions. The results showed that the relationship between anthropogenic dusts and population is more obvious for croplands than for other land cover types (crop mosaics, grassland, and urbanized regions). The production of anthropogenic dust increases as the population density grows to more than 90 persons $km^{-2}$. The most significant relationship between anthropogenic dust and population occurred in an Indian semi-arid region that had a high portion of croplands, and the peak anthropogenic dust probability appeared at a 220 persons $km^{-2}$ population density and a 60 person $km^{-2}$ population change.

In earlier publications (Tegen and Fung, 1995; Huang et al., 2015), anthropogenic dusts were described at the portion of mineral dust that is primarily produced by various human activities on disturbed soils (e.g., agricultural practices, industrial activity, transportation, desertification and deforestation). East Asia has the highest concentration of anthropogenic aerosols in the world (Sugimoto et al., 2015a). Additionally, East Asia is a unique region wherein mineral dust (Asian dust) sources are located near urban and industrial areas. During transportation, dust often mixes with anthropogenic aerosols (Takemura et al., 2002) and induces new environmental and climatic problems (Su et al., 2008). In this paper, we attempt to study this kind of transported anthropogenic dust (TDU), which is mainly dominated by dust and could be mixed with other anthropogenic aerosol types. Although there are some quantitative assessments about the anthropogenic dust, the accuracies of these results are still unknown due to the limited data and preliminary detection methods. In Huang's method (Huang et al, 2015), approximately 9.6% of the anthropogenic dust is misclassified as natural dust, and 8.7% of the natural dust is misclassified as anthropogenic dust within the PBL (planetary boundary layer).

Lidar, an advanced active remote sensing instrument with high spatial and temporal resolutions and high accuracy detection abilities in the lower altitudes, has become an important technology for detecting the spatial and temporal distributions of the aerosol physical properties (Zhou et al, 2013). Hua et al. (2005a, 2005b, 2005c, 2005d, 2007) used ultraviolet Rayleigh–Mie Lidar and Raman Lidar for temperature profiling of the troposphere. Chen et al. (2010) and Liu et al. (2011) used the satellite-based Lidar CALIOP (Cloud-Aerosol Lidar with Orthogonal Polarization) to detect the dust layers with fewer misclassifications. However, when detecting surface dusts, ground-based Lidar has an obvious advantage over the satellite-based Lidar. In this study, the ground-based Lidar measurements are used to validate the thresholds used in the CALIPSO CAD algorithm (Liu et al., 2005). The total attenuated backscattering coefficient at 532 nm, the linear volume depolarization ratio and the color ratio are derived from the L2S-SM-II dual-band polarization Lidar developed by the NIES (National Institute for Environment Studies) and provided at the Semi-Arid Climate and Environment Observatory of Lanzhou University (SACOL).

The paper is arranged as follows. The details of the datasets used are given in section 2. In section 3, the inversion and detection method used in this study is introduced. Examples of distinguishing pure dust and transported anthropogenic dust using multiple measurements are presented in section 4. A comparison of the optical properties of two dust cases is presented in section 5. The conclusion and discussion are presented in section 6.

## 2 Data

### 2.1 Surface station data

The global surface weather data set from the China Meteorological Administration State Information Center was used in this study. This data set is based on the global surface monthly data and real-time data, which are then decoded and normalized. The time period of the data set spans from January 1, 1980 to June 1, 2015. There are 65 elements in every record of the data set, and the types of variables are set as characters. The data set is strictly quality controlled. Here, we analyze the weather phenomena from October 2009 to June 2013.

### 2.2 Ground-based Lidar data

The Semi-Arid Climate and Environment Observatory of Lanzhou University

(SACOL) (Huang et al., 2008, Guan et al., 2009, Wang et al., 2010, Huang et al., 2010, Bi et al., 2010, Liu et al., 2011), built in 2006, is situated on the Loess Plateau (35.946 °N, 104.137 °E) at approximately 1965.8 m above sea level. The topography around the site is characterized by the Loess Plateau and consists of plains, ridges and mounds, etc. The dominant species within the immediate area of the study site are Stipa bungeana as well as Artemisia frigida and Leymus secalinus. SACOL is approximately 48 km away from the center of Lanzhou. The terrain where the measurements are made is flat and covered with short grasses. The reason that the site was built on the mountain top is as follows: the environment of the mountain top is almost completely natural and is rarely affected by human activity and the climate at the site can represent that of the surrounding hundreds of kilometers. Thus, by building at the top of the mountain, the influences of houses and other human activities are avoided. The L2S-SM-II dual-band depolarization Lidar are operated at SACOL and began observing aerosols and clouds in October 2009.

Fig. 2 shows the structure of the L2S-SM-II dual-band depolarization Lidar at SACOL, which is a two-wavelength polarization-sensitive backscatter Lidar. The NIES's vertically resolved aerosol and cloud measurements will enable new insights into the roles of aerosols and clouds in the Earth's climate system. This Lidar system consists of three parts: the laser source, signal receipt-system and data recording device. The laser source is a flash lamp pumped Nd:YAG laser device. Two laser beams (with wavelengths of 532 nm and 1064 nm) are shot into the atmosphere to calibrate for the beam expanding, and the return signal is received by the Cassegrain

Atmos. Chem. Phys. Discuss., https://doi.org/10.5194/acp-2017-1000
Manuscript under review for journal Atmos. Chem. Phys.
Discussion started: 14 December 2017


telescope with a diameter of 20 cm. The perpendicular and parallel components of the 532 nm backscatter signal are received by two detectors. Thus, we can derive polarization information. Using the relationship of the delay time and the height at which the light is scattered, the power of the return signal and the concentrations of atmospheric aerosols are known. Therefore, the vertical profile of the optical properties of aerosols can be derived (Zhou et al, 2013). The vertical resolution of the Lidar structure is 6 m and can reach a height of 18 km above the ground. The time resolution of the Lidar system is 15 min. For our study, we choose measurements taken over a continuous period from October 2009 to June 2013.

## 3 Retrieval and detection methods

Lidar signals, such as the total attenuated backscattering coefficient at 532 nm, linear volume depolarization ratio, and color ratio, reflect the physical and optical properties of aerosols and clouds. There are a number of effective methods for deriving particulate extinction and backscatter coefficients from calibrated, range-corrected Lidar signals. Among these, the most widely used are the Klett method (Klett, 1985), the Fernald method (Fernald, 1984) and the so-called linear iterative method first introduced in the late 1960s (Elterman, 1966) that was subsequently extensively used by Platt (Platt, 1973; Platt et al., 1998). The Fernald algorithm was originally developed within the context of single scattering. In later years, both algorithms were adapted for use in multiple scattering analyses via a correction factor of the range-resolved extinction coefficients (e.g., as in (Young, 1995)). In our study, we adapt the Fernald method.

Generally, clouds are seen to have larger backscatter coefficients and higher color ratios (~ 1) than aerosols. The exceptions to this general rule are desert aerosols and maritime aerosols under high relative humidity conditions, both of which then exhibit relatively large color ratios. These scattering features can be used to distinguish aerosols from clouds. Additionally, the linear volume depolarization ratio is a useful indicator for identifying irregular particles and provides a means of discriminating ice clouds from water clouds and identifying dust aerosols. An attenuated backscattering coefficient is vital in many aspects. Accurate aerosol and cloud heights and the retrieval of extinction coefficient profiles are all derived from the total backscatter measurements. Winker et al (2006) compared the sensitivities of the 532 nm and 1064 nm channels. The APD detector used in the 1064 nm channel has much higher dark noise than the PMT detectors used in the 532 nm channels. The sensitivity of the 1064 nm channel is limited in most situations by the detector dark current, so the sensitivity shows much smaller variations between days and nights and over varying altitudes than the 532 nm channel. For this reason, the attenuated backscattering coefficient at 532 nm is one of the best indicators for discriminating aerosols and clouds.

The linear volume depolarization ratio is defined as the perpendicular components of the 532 nm attenuated backscatter coefficient over the parallel components of the same coefficient. The expression for this is as follows:

$$\delta(r) = \beta_{532,\perp}(r)/\beta_{532,\parallel}(r) \quad (1)$$

The sphericity of a particle is represented by its linear volume depolarization ratio, such that a value near 0 indicates that the particle is nearly spherical, while a large value indicates that the particle is aspherical. The linear volume depolarization of ice crystals is typically in the range of 30%-50% but depends on the crystal shape and aspect ratio. Lower values can be seen when horizontally oriented particles are present (Sassen and Benson, 2001). In contrast, the backscattering from spherical water droplets preserves the polarization of the incident light, so the value of the linear volume depolarization ratio is near 0. We note that the linear volume depolarization ratio is predominantly influenced by the sphericity of the dust particles (e.g., Ansmann et al., 2003). Therefore, the polarization is sensitive to aspherical particles, such as ice and dust. In a large number of studies, depolarization acts as a criteria to distinguish clouds, aerosols, cloud phases, and aerosol types, especially for dust.

The color ratio is defined as the ratio of the backscatter coefficient at 1064 nm to that of 532 nm. The expression for this is as follows:

$$\mathrm{x(r)} = \beta_{1064}(\mathrm{r})/\beta_{532}(\mathrm{r}) \quad (2)$$

The color ratio is an indicator of the particle size. A large value represents a large particle, and a small value represents a small particle. The color ratio is an indicator of the particle's variable scattering of light across the available spectra and can be used to distinguish clouds, aerosols and type of clouds. Meanwhile, the color ratio represents the particle size. When the color ratio is large, the radius of the particle is large, otherwise the radius is small. The color ratio is sensitive to the particle orientation, particle shape and particle size. Because the Lidar coefficients at 532 nm and 1064 nm are different, the color ratios derived from these coefficients show some difference from those of other studies.

When considering the Lidar signal, the general rules used in these classifications are as follows: if the linear volume depolarization ratio is high, then the layer is dust dominated; if the linear volume depolarization ratio is low and the color ratio is high, then the layer is pollution dominated; and if the linear volume depolarization ratio is somewhere in the middle and the color ratio is high, the layer should be a mixture of dust and pollution (and possibly other types of aerosols) (Liu et al., 2008b).

Then, according to the surface weather record and boundary layer height, a subtype of dust aerosols (pure dust or transported anthropogenic dust) can then be identified. According to the maximum standard deviation technique first developed by Jordan et al. (2010), the PBL is derived using the NIES 532-nm attenuated backscatter. Liu et al. (2015) proved that the results of the PBL height values derived from the NIES Lidar were coincident with the ECMWF observations. Because the dust events always occurred within the PBL and the long-range transportation related to the westerly wind occurred above the PBL, the transported anthropogenic dust is above the PBL, and the pure dust is within the PBL. The main cases of the pure dust and transported anthropogenic dust are listed as follows. Case I: if there exists floating dust, blowing dust or dust storms in the records of the surface weather stations and the dust layer is within the PBL, the dust is regarded as pure dust. Case II: if there is no relation of the dust to the surface weather record and the dust layer is above the PBL,

Atmos. Chem. Phys. Discuss., https://doi.org/10.5194/acp-2017-1000
Manuscript under review for journal Atmos. Chem. Phys.
Discussion started: 14 December 2017


the dust layer is also regarded as pure dust that has been transported during long-range prevailing winds. Case III: if there is no relation of the dust to the surface weather record and the dust layer is in the PBL, the dust layer is regarded as transported anthropogenic dust that has been transported to the SACOL station and mixed with other anthropogenic aerosols during its transport.

From October 2009 to June 2013, there are 40 days and 451 days showing pure dust and transported anthropogenic dust, respectively, and the sample numbers are 2709 and 32203, respectively.

## 4 Case studies

### 4.1 Pure dust case

As shown in Fig. 2, Lidar signals from the L2S-SM-II dual-band polarization Lidar of SACOL together with HYSPLIT MODEL were used to distinguish the types of dust. Lidar signals dependent on height and time were used to distinguish dust from clouds and air molecules. The values of the attenuated backscatter coefficient, linear volume depolarization ratio and color ratio of the dust are smaller than those of clouds and greater than those of air molecules. Therefore, dust is separated from clouds and air molecules. Then, the back trajectories from the HYSPLIT MODEL were used to show the origins of the dust. By introducing the PBL derived from the backscatter coefficient at 532 nm, we can regard dust within the PBL from the source regions as pure dust, while the dust above the PBL is from cities, croplands and other anthropogenic land surfaces and is transported anthropogenic dust. Lüthi et al. (2014) believed that the attenuated backscatter coefficients at 532 nm were located within the

Atmos. Chem. Phys. Discuss., https://doi.org/10.5194/acp-2017-1000
Manuscript under review for journal Atmos. Chem. Phys.
Discussion started: 14 December 2017


Atmospheric Chemistry and Physics Discussions

ranges of 0.0008-0.0016/km/sr, 00016-0.0044/km/sr and 0.0044-0.0072/km/sr, corresponding to low, medium, and high aerosol concentrations. On the basis of CALIPSO's algorithm, aerosols whose linear volume depolarization ratios are greater than 0.075 were identified as dust (Liu et al., 2005).

Fig. 3 presents the dust case measured by the NIES Lidar on 19 October 2009. The heights in Fig. 3 and Fig. 5 are the heights above ground level. Generally, the NIES Lidar products indicate aerosols with green-yellow-orange color schemes and clouds with white-gray color schemes. As show in Fig. 3, a layer (dust layer) is detected at the height of 0-3 km. The total attenuated backscattering coefficient at 532 nm, and the linear volume depolarization ratio range from 0.0015-0.006/km/sr and 0.06-0.3, respectively, which indicate that dust particles are the main components of this layer. Additionally, there is floating dust in the surface weather record. The black dotted line indicates the PBL heights. As shown in Fig. 3, the dust layer is within PBL. Therefore, the dust layer in this case is regarded as pure dust.

Additionally, three-day-back-trajectory simulations produced with the HYSPLIT-4 model have been used to explore the most likely sources and transportation routes of the dust events. The HYSPLIT-4 transport model (fourth-generation of HYSPLIT model) provided by the NOAA Air Resources Laboratory is used to calculate the simple air-parcel trajectories with interpolated meteorological fields. The 6-h-interval final archive data are generated from the NCEP (National Centers for Environmental Prediction) Global Data Assimilation System (GDAS) reanalysis 3-dimensional meteorological fields. According to the results, if dust aerosols from deserts are directly transported to SACOL by the westerly winds, these dust aerosols are classified as pure dust. Otherwise, if they are transported by easterly winds, the dust aerosols will pass through some cities and be heavily influenced by human activities. In these circumstances, the dust aerosols from the dust source regions would mix with urban pollution from other local areas; thus, the mixture is classified as transported anthropogenic dust.

The result of the back-trajectory simulations of this case is shown in Fig. 4. The dust trajectory starts at SACOL and is marked with a black star. The trajectories are marked with different colors indicating starting points at different altitudes, and the altitudes of the air-entrained dust particles during their transport are provided at the bottom of Fig. 4. The dust aerosols detected at SACOL originate from the neighboring Taklamakan Desert. During their transportation, few human activities are present in their pathway. Combined with Fig. 3 and the surface weather record, these results suggest that the aerosols are pure dust.

**4.2 Transported anthropogenic dust case**

Similarly, Fig. 5 presents the dust case measured by the NIES Lidar on 31 July 2010. As shown in Fig. 5, a dust layer is detected at a height of 0-2 km. The total attenuated backscattering coefficient at 532 nm and the linear volume depolarization ratio range from 0.0015-0.006/km/sr and 0.06-0.3, respectively, which indicate that dust particles are the main components of this layer. Additionally, there is no related record from the surface weather record. The black dotted line in Fig. 5 indicates the PBL height. Thus, we can see that the dust layer is within the PBL. Therefore, the dust layer is classified as transported anthropogenic dust.

The back-trajectory simulation is shown in Fig. 6 and suggests that the dust aerosols detected at SACOL originated from Mongolia. During their transport, there were many human activities that occurred along their path over Baotou and Yulin cities. Taking into account the weather conditions and observation times combined with Fig. 3 confirms that these aerosols are transported anthropogenic dust that were mixed with anthropogenic emissions from cities.

## 5. Comparison of the optical properties of two types of dust

A histogram of the linear volume depolarization ratios of pure dust and transported anthropogenic dust is shown in Fig. 7. The statistical results of the frequency distributions of the linear volume depolarization ratios for pure dust and transported anthropogenic dust show that the mean depolarization ratios of pure dust and transported anthropogenic dust are 0.249 and 0.173, respectively; the skewness coefficients are 1.315 and 0.038 for transported anthropogenic dust and pure dust, respectively; and the kurtosis coefficients are -0.504 and 0.971 for transported anthropogenic dust and pure dust, respectively. Additionally, the peak values are approximately 0.275 for pure dust and approximately 0.095 for transported anthropogenic dust. Freudenthaler et al. (2009) and Wandinger et al. (2010) both found that the particle linear depolarization ratio was approximately 0.3 during SAMUM–1 and SAMUM–2, respectively, which is consistent with our results. From the results above, we can see that the depolarization of pure dust is greater than that of transported anthropogenic dust, which means that pure dust is more spherical. The reason why the depolarization of pure dust is greater than that of transported anthropogenic dust is that during its transportation, dust is mixed with smoke or anthropogenic aerosols, which makes the mixed aerosol nearly spherical. Specifically, the results show that during its transportation, dust can be fully mixed with inorganic salt (Sun et al., 2005; Shen et al., 2007; Fan et al., 1996), pollution elements such as Se, Ni, Pb, Br, Cu (Zhang et al., 2005), black carbon (Kim et al., 2004), VOCs and polyaromatic hydrocarbon (Hou et al., 2006), thus becoming anthropogenic dust.

If there is a threshold to distinguish pure dust and transported anthropogenic dust, the total frequency whose linear volume depolarization ratio is larger than the threshold is considered to be a misclassification for transported anthropogenic dust, and those smaller than the threshold are considered to be a misclassification for pure dust. In this way, a 0.2 linear volume depolarization ratio could be used as a threshold for distinguishing pure dust and transported anthropogenic dust in other detections. Using this simple classification, the misclassifications of pure dust and transported anthropogenic dust are 27.6% and 28.0%, respectively. Meanwhile, the total misclassification remains at a low level. Although most of the pure dust and transported anthropogenic dust can be classified using the linear volume depolarization ratio threshold, the overlapping value between 0.16 and 0.23 may indicate ambiguous values for distinguishing pure dust and transported anthropogenic dust via the linear volume depolarization ratio approach alone. Some effort is needed to reduce misclassification.

Happily, this threshold is consistent with that of CALIPSO (Liu et al., 2005), but is slightly smaller than the 0.23 from the results of Huang et al. (2015). In his research, different dust aerosols were distinguished based on their geographic locations, namely, dust aerosols (including pure dust and transported anthropogenic dust) from northern China are classified as transported anthropogenic dust, and dust aerosols from the Taklamakan Dessert are classified as natural dust. In this case, anthropogenic dust is a part of natural dust and is influenced by human activity. During its long-range transport, anthropogenic dust would mix with other aerosols and absorb water vapor in the air. Therefore, the transported anthropogenic dust is more spherical than the anthropogenic dust in northern China. Additionally, our results concerning the linear volume depolarization ratio are smaller than those of Huang et al. (2015).

A histogram distribution of the color ratios for pure dust and transported anthropogenic dust is shown in Fig. 8. The statistical results indicate that the mean color ratios for pure dust and transported anthropogenic dust are 0.8 and 1.2, respectively. The skewness coefficients are 2.9 and 2.1 for transported anthropogenic dust and pure dust, respectively, and the kurtosis coefficients are 10.6 and 6.5 for transported anthropogenic dust and pure dust, respectively. There are two peaks for pure dust, the larger of which is 0.8, which represents the large dust particles in the local areas during dusty days. The smaller one is 0.25, which represents the smaller dust particles transported from the remote dust sources. The peak value for the transported anthropogenic dust is approximately 0.5. From these results, we can see that the color ratio of the transported anthropogenic dust is generally greater than that of the pure dust, which means that the transported anthropogenic dust is larger. The reason why the color ratio of transported anthropogenic dust is greater than that of pure dust is that the dust is mixed with smoke or anthropogenic aerosols during its transport, causing slight growth of the mixed aerosol. In the source regions, the color ratios of dust particles are between 0.7-1.0 (Huang et al., 2007; He et al., 2015). Huang et al. (2007) found the mean color ratio of the frequently observed dust aerosols at heights of 4-7 km over the Tibet Plateau in the summer to be 0.83.

Zhou et al. (2013) found the relationship between the layer-integrated attenuated backscattering coefficient and the layer-integrated depolarization ratio to distinguish dusts, water clouds and ice clouds. Single scatterings by water droplets do not depolarize backscattered light, but multiple scattering events do tend to depolarize Lidar signals within water cloud. Thus, the layer-integrated depolarization ratios of water clouds show considerably large values and increase with the layer-integrated attenuated backscattering coefficient. The ice cloud that contains a large number of randomly oriented ice particles corresponds to small attenuated backscattering coefficients and high depolarization ratio values, while those containing horizontally oriented ice crystals that could lead the presence of specular reflections show high attenuated backscattering coefficients and small depolarization ratios. Dust is more widely distributed with low backscattered light values and a wide range of depolarization ratios. The obviously different distributions of dusts, water clouds, and ice clouds can be used to identify these features. Here, we attempt to find the attenuated backscattering coefficient and linear volume depolarization ratio relationship between pure dust and transported anthropogenic dust. Fig. 9 and Fig. 10

Atmos. Chem. Phys. Discuss., https://doi.org/10.5194/acp-2017-1000
Manuscript under review for journal Atmos. Chem. Phys.
Discussion started: 14 December 2017


depict the relationship between the attenuated backscattering coefficient and linear volume depolarization ratio as well as the attenuated backscattering coefficients and color ratios for pure dust and transported anthropogenic dust.

Fig. 9 shows the percentage of occurrences of pure dust and transported anthropogenic dust in a 0.02*0.0008/km/Sr pixel. As shown in Fig. 9, the range of attenuated backscattering coefficients is 0.0009 – 0.0073 /km/Sr and the range of linear volume depolarization ratios is 0.06 – 0.42 for both pure dust and transported anthropogenic dust. The distribution of pure dust seems to be symmetric, and the axis of symmetry is at about x=0.26. The pure dust is concentrated in the middle-right section, indicating that the attenuated backscattering coefficient and linear volume depolarization ratio are relatively large. In contrast, the distribution of transported anthropogenic dusts also seem to be symmetric, and the axis of symmetry is a straight line whose slope is approximately 0.015. The transported anthropogenic dust is concentrated in the lower-left corner, which means that the attenuated backscattering coefficient and linear volume depolarization ratio are relatively small. Compared with the distribution of peaks for pure dust, that for transported anthropogenic dust is obviously shifted to the left. Among these peaks for pure dust, the minimum and maximum values of the linear volume depolarization ratios are 0.16 and 0.34, respectively, while for transported anthropogenic dust, the minimum and maximum values of the linear volume depolarization ratios are 0.08 and 0.18, respectively. The linear volume depolarization ratio of pure dust is greater than that of transported anthropogenic dust, and the overlapping section is very small.

Atmos. Chem. Phys. Discuss., https://doi.org/10.5194/acp-2017-1000
Manuscript under review for journal Atmos. Chem. Phys.
Discussion started: 14 December 2017


Next, we attempt to find the attenuated backscattering coefficient and color ratio relationship for pure dust and transported anthropogenic dust and then use it to detect different dust aerosols from satellite observations. Fig. 10 shows the percentage of occurrences of pure dust and transported anthropogenic dust in a 0.1*0.0008 pixel. As shown in Fig. 10, the range of attenuated backscattering coefficients is 0.0009 – 0.0057 /km/Sr and the range of color ratios is 0.1 – 1.5 for both pure dust and transported anthropogenic dust. However, the obvious difference is that the range of the color ratios for pure dust is not wider than that of transported anthropogenic dust. The distribution of pure dust seems to be symmetric, and the axis of symmetry is a straight line. The pure dust is concentrated in two sections (the upper-left portion and lower-right portion), indicating that when the color ratio is small, the attenuated backscattering coefficient is large, and when the color ratio is large, the attenuated backscattering coefficient is small. The two sections observed for pure dust correspond to small dust particles transported from remote source regions and large particles transported from local areas. In contrast, the distribution of the transported anthropogenic dust also seems to be symmetric, and the axis of symmetry is a straight line whose slope is less than that for pure dust. The transported anthropogenic dust distribution is concentrated in the lower-middle zone, indicating that the attenuated backscattering coefficient is relatively small, and the color ratio is near the middle of the possible values. Compared with the distribution of extremes for pure dust, that for transported anthropogenic dust is distinctly set in the middle. Among those extrema for pure dust located in the upper-left portion of the distribution, the minimum and maximum values of the color ratios are 0.2 and 0.4, respectively, and those for pure dust located in the lower-right portion of the distribution show minimum and maximum values of the color ratios are 0.7 and 0.9, respectively. Meanwhile, for the transported anthropogenic dust, the minimum and maximum values of the color ratios are 0.4 and 0.6, respectively. On average, the color ratios of the transported anthropogenic dust are greater than those of pure dust.

## 6 Conclusions and discussion

As we discussed above, pure dust and transported anthropogenic dust can be distinguished by using a combination of ground-based L2S-SM-II dual-band polarization Lidar data, surface weather station records and PBL heights. Contrasting the frequency distributions of the linear volume depolarization ratios of two different kinds of dust, we find the following: the mean linear volume depolarization ratios of pure dust and transported anthropogenic dust are 0.249 and 0.173, respectively; the maximum linear volume depolarization ratios of pure dust and transported anthropogenic dust are 0.275 and 0.095, respectively. The mean value of pure dust is greater than that of anthropogenic dust, which means that the pure dust is more spherical, and based on the relationship of misclassification of pure dust and transported anthropogenic dust verses depolarization, a threshold of 0.2 is chosen to classify the two different kinds of dust. By contrasting the frequency distribution of the color ratios of two different kinds of dust, we find the following: the mean color ratios of pure dust and transported anthropogenic dust are 0.8 and 1.2, respectively; the maximum value of the color ratio of transported anthropogenic dust is 0.5, but

Atmos. Chem. Phys. Discuss., https://doi.org/10.5194/acp-2017-1000
Manuscript under review for journal Atmos. Chem. Phys.
Discussion started: 14 December 2017


there are two maxima for pure dust: the smaller is 0.25, and the larger is 0.8. The mean value of the transported anthropogenic dust is greater than that of pure dust, which means that transported anthropogenic dust is larger. The results of the relationship between the attenuated backscattering coefficient and the linear volume depolarization ratio of pure dust and transported anthropogenic dust show that the transported anthropogenic dust is concentrated in the lower-left corner of the overall distribution, which means the linear volume depolarization ratio is relatively small; in contrast, the pure dust is concentrated in the right section of its distribution, implying that the linear volume depolarization ratio is relatively large. The results of the relationship between the attenuated backscattering coefficient and the color ratio of pure and transported anthropogenic dusts show that there are two maxima for pure dust: one is shown in the upper-left portion of Fig. 10 and corresponds with a small color ratio and a large attenuated backscattering coefficient, while the other is shown in the lower-right portion of Fig. 10 and corresponds with a large color ratio and small attenuated backscattering coefficient. The two peaks of pure dust represent the small dust particles transported from the remote source regions by the prevailing wind and the large particles transported from local areas during dusty days. However, the color ratio and attenuated backscattering coefficient for the transported anthropogenic dust are uniformly distributed.

The dust particles transported by the prevailing winds are relatively small and spherical, while the dust particles transported during dusty days are relatively large and aspherical. If there are no dust events in the local regions, the dust particles are usually transported anthropogenic dust. Therefore, the transported anthropogenic dusts are relatively large and, owing to mixing with other types of aerosols or anthropogenic pollution, these dust particles have relatively regular shapes (Huang et al., 2007).

Xie et al. (2008) continuously measured aerosol optical properties with the NIES compact Raman Lidar over Beijing, China, from 15 to 31 December 2007. Their results indicated that the total linear volume depolarization ratio was mostly below 10% during a pollution episode, whereas it was greater than 20% during the Asian dust episode. The average total linear volume depolarization ratio of the nonspherical mineral dust particles was 19.54±0.53%.

Huang et al. (2010) conducted an intensive spring aerosol sampling campaign over northwestern and northern China as well as over a megacity in eastern China during the spring of 2007 to investigate the mixing of Asian dusts with pollution aerosols during their long-range transports. The western dusts were less polluted than the other two dust sources. The western dusts contained relatively small amounts of anthropogenic aerosols and were mainly derived from the Taklimakan Desert, which is a paleomarine source. The northwestern dust had considerable chemical reactivities and mixings with the sulfur precursors emitted from the coal mines along the path of their long-range transport. The northeastern dust that reached Shanghai had high acidity and became a mixed aerosol via its interactions with other dust, local pollutants, and sea salts.

Asian dust is often mixed with air pollution aerosols during its transport.

Sugimoto et al. (2015b) studied the internally mixed Asian dust with air pollution aerosols using a polarization optical particle counter and a polarization-sensitive two-wavelength Lidar. The results showed that the backscattering linear volume depolarization ratio was smaller for all particle sizes in polluted dust. The backscattering color ratio of the polluted dust was comparable to that of pure dust, but the linear volume depolarization ratio was lower for polluted dust. In addition, coarse nonspherical particles (Asian dust) almost always existed in the background, and the linear volume depolarization ratio showed seasonal variations with a lower linear volume depolarization ratio in the summer. These results suggest that background Asian dust particles are internally mixed during the summer.

With the help of surface weather station data, observations and PBL heights, Lidar data can be used to identify pure dust and transported anthropogenic dust via their optical properties. Then, the optical properties of pure dust and transported anthropogenic dust can be analyzed. Last, by combining the linear volume depolarization ratio–attenuated backscattering coefficient relationship, the color ratio–attenuated backscattering coefficient relationship, the threshold for the linear volume depolarization ratio and the peak values for the color ratios, our ability to identify different dust aerosols will be greatly improved. Studies of the optical properties of pure dust and transported anthropogenic dust using ground-based Lidar would be highly beneficial for detecting dust using satellite data and would improve our ability to model dust. Thus, these studies can improve our understanding of the impacts of Asian dust on regional and global climate change as well as providing information to

Atmos. Chem. Phys. Discuss., https://doi.org/10.5194/acp-2017-1000
Manuscript under review for journal Atmos. Chem. Phys.
Discussion started: 14 December 2017




help estimate the influence of human activities on the climate system.

***Acknowledgements.*** Supported by the National Fund Committee Innovation Group (Grant No. 41521004), General Program (Grant No. 41775021), National Natural Science Foundation of China (Grant No. 41305026) and the National Natural Science Foundation of China (Grant No. 41375032). Ground-based Lidar data was obtained from the Semi-Arid Climate and Environment Observatory of Lanzhou University (SACOL). The surface station weather data were obtained from the China Meteorological Data Sharing Service System.

Atmos. Chem. Phys. Discuss., https://doi.org/10.5194/acp-2017-1000
Manuscript under review for journal Atmos. Chem. Phys.
Discussion started: 14 December 2017


Atmospheric Chemistry and Physics Discussions
Open Access
EGU

## References

Ansmann, A., Bösenberg, J., Chaikovsky, A., Comerón, A., Eckhardt, S., Eixmann, R., Freudenthaler, V., Ginoux, P., Komguem, L., Linné, H., López Márquez, M. Á., Matthias, V., Mattis, I., Mitev, V., Müller, D., Music, S., Nickovic, S., Pelon, J., Sauvage, L., Sobolewsky, P., Srivastava, M., Stohl, A., Torres, O., Vaughan, G., Wandinger, U., and Wiegner, M., Long-range transport of Saharan dust to northern Europe: The 11–16 October 2001 outbreak observed with EARLINET, J. Geophys. Res., 108, 4783, doi:10.1029/2003JD003757, 2003.

Bi, J., Huang, J., Fu. Q., Wang, X., Shi, J., Zhang, W., Huang Z., and Zhang B.: Toward characterization of the aerosol optical properties over Loess Plateau of Northwestern China, J. Quant. Spectrosc. Ra., 112, D00K17, doi:10.1029/2009JD013372, 2010.

Chen, B., Huang, J., Minnis, P., Hu, Y., Yi, Y., Liu, Z., Zhang, D., and Wang, X.: Detection of dust aerosol by combining CALIPSO active lidar and passive IIR measurements, Atmos. Chem. Phys., 10, 4241-4251, doi: 10.5194/acpd-10-3423-2010, 2010.

Elterman, L.: Aerosol measurements in the troposphere and stratosphere, Appl. Opt., 5, 1769-1776, 1966.

Fan, X.., Okada, K., Niimura, N., Kai, K., Arao, K., and Shi, G.: Mineral particles collected in China and Japan during the same Asian dust-storm event, Atmos. Environ., 30, 347-351, doi: 10.1016/1352-2310(95)00271-Y, 1996.

Fernald, F.: Analysis of atmospheric lidar observations-Some comments, Appl. Opt., 23, 652-653, doi: 10.1364/AO.23.000652, 1984.

Freudenthaler, V., Esselborn, M., Wiegner, M., Heese, B., Tesche, M., Ansmann, A., Müller, D., Althausen, D., Wirth, M., Fix, A., Ehret, G., Knippertz, P., Toledano, C., Gasteiger, J., Garhammer, M. and Seefeldner, M.: Depolarization ratio profiling at several wavelengths in pure Saharan dust during SAMUM 2006, Tellus B, 61, 165-179, doi: 10.1111/j.1600-0889.2008.00396.x, 2009.

Guan, X., Huang, J., Guo, N., Bi, J., and Wang, G..: Variability of soil moisture and its relationship with surface albedo and soil thermal parameters over the Loess Plateau, Adv. in Atmos. Sci., 26(9), 692-700, doi: 10.1007/s00376-009-8198-0, 2009.

Guan, X., Huang, J., Zhang, Y., Xie, Y., and Liu, J.: The relationship between anthropogenic dust and population over global semi-arid regions, Atmos. Chem. Phys., 16, 5159-5169, doi:10.5194/acp-16-5159-2016, 2016.

He, Y. and Yi, F.: Dust Aerosols Detected Using a Ground-Based Polarization Lidar and CALIPSO over Wuhan (30.5 °N, 114.4 °E), China, Adv. in Meteor., 2015, Article ID 536762, 18 pp., doi:10.1155/2015/536762, 2015.

Hou, X., Zhuang, G., Sun, Y., and An, Z.: Characteristics and sources of polycyclic aromatic hydrocarbons and fatty acids in PM 2.5 aerosols in dust season in China, Atmos. Environ., 2006, 40, 3251-3262, doi:10.1016/j.atmosenv.2006.02.003, 2006.

Hua, D., and Kobayashi, T.: Ultraviolet Rayleigh-Mie lidar by use of a multicavity Fabry-Perot filter for accurate temperature profiling of the troposphere, Appl. Optics, 2005a, 44(30), 6474-6478.

Hua, D., Uchida, M., and Kobayashi, T.: Ultraviolet Rayleigh-Mie lidar for daytime-temperature profiling of the troposphere, Appl. Optics, 2005b, 44(7), 1315-1322.

Hua, D., Uchida, M., and Kobayashi, T.: Ultraviolet Rayleigh-Mie lidar with Mie-scattering correction by Fabry-Perot etalons for temperature profiling of the troposphere, Appl. Optics, 2005c, 44(7), 1305-1314.

Hua, D., and Kobayashi, T.: UV Rayleigh–Mie Raman lidar for simultaneous measurement of atmospheric temperature and relative humidity profiles in the troposphere, Jap. J. Appl. Phys., 2005d, 44(3R), 1287.

Hua, D., Liu, J., Uchida, K., and Kobayashi, T.: Daytime temperature profiling of planetary boundary layer with ultraviolet rotational Raman lidar, Jap. J. Appl. Phys., 2007, 46(9R), 5849.

Huang, J., Fu, Q., Su, J., Tang, Q., Minnis, P., Hu, Y., Yi, Y., and Zhao, Q.: Taklimakan dust aerosol radiative heating derived from CALIPSO observations using the Fu-Liou radiation model with CERES constraints, Atmos. Chem. Phys., 9, 4011-4021, doi:10.5194/acp-9-4011-2009, 2009.

Huang, J., Wang, T., Wang, W., Li, Z., and Yan, H.: Climate effects of dust aerosols over East Asian arid and semiarid regions, J. Geophys. Res., 119, 11398-11416, doi:10.1002/2014JD021796, 2014.

Huang, J., Ge, J., and Weng, F.: Detection of Asia dust storms using multisensor satellite measurements, Remote Sens. Environ., 110, 186-191, doi: 10.1016/j.rse.2007.02.022, 2007.

Huang, J., Lin, B., Minnis, P., Wang, T., Wang, X., Hu, Y., Yi, Y., and Ayers, J.: Satellite-based assessment of possible dust aerosols semi-direct effect on cloud water path over East Asia, Geophys. Res. Lett., 33, L19802, doi:10.1029/2006GL026561, 2006b.

Huang, J., Liu, J., Chen, B., and Nasiri, S.: Detection of anthropogenic dust using CALIPSO lidar measurements, Atmos. Chem. Phys., 15(20), 11653-11665, 2015.

Huang, J., Minnis, P., Lin, B., Wang, T., Yi, Y., Hu, Y., Sun-Mack, S., and Ayers, J.: Possible influences of Asian dust aerosols on cloud properties and radiative forcing observed from MODIS and CERES, Geophys. Res. Lett., 33, L06824, doi:10.1029/2005GL024724, 2006a.

Huang, J., Minnis, P., Lin, B., Yi, Y., Khaiyer, M., Arduini, R., and Mace, G.: Advanced retrievals of multilayered cloud properties using multispectral measurements, J. Geophys. Res., 110, D15S18, doi:10.1029/2004JD005101, 2005.

Huang, J., Zhang, W., Zuo, J., Bi, J., Shi, J., and Wang, X.: An overview of the semi-arid climate and environment research observatory over the Loess Plateau, Adv. Atmos. Sci., 25, 906-921, doi: 10.1007/s00376-008-0906-7, 2008.

Huang, K., Zhuang, G., Li, J., Wang, Q., Sun, Y., Lin, Y., and Fu, J. S.: Mixing of Asian dust with pollution aerosol and the transformation of aerosol components during the dust storm over China in spring 2007, J. Geophys. Res., 115, D7, 2010.

Huang, Z., J. Huang, J., Bi, J., Wang, G., Wang, W., Fu, Q., Li, Z., Tsay, S., and Shi, J.: Dust aerosol vertical structure measurements using three MPL lidars during 2008 China-U.S. joint dust field experiment, J. Geophys. Res.,115, D00K15, doi:10.1029/2009JD013273, 2010.

Jordan, N., Hoff, R., and Bacmeister, J.: Validation of goddard earth observing system-version 5 MERRA planetary boundary layer heights using CALIPSO, J. Geophys. Res., 115, 2010.

Kim, K., He, Z., and Kim, Y.: Physicochemical characteristics and radiative properties of Asian dust particles observed at Kwangju, Korea, during the 2001 ACE-Asia intensive observation period, J. Geophys. Res., 109, D19, doi: 10.1029/2003JD003693, 2004.

Klett, J., Lidar inversion with variable backscatter/extinction ratios, Appl. Opt., 24, 1638-1643, 1985

Li, Z.: Aerosol and climate: a perspective over East Asia, in observation, theory, and modeling of the atmospheric variability, World Sci. Co., Singapore, 501–525, doi:10.1142/9789812791139_0025, 2004.

Liu, J., Huang, J., Chen, B., Zhou, T., Yan, H., Jin, H., Huang, Z. and Zhang, B.: Comparisons of PBL heights derived from CALIPSO and ECMWF reanalysis data over China, Journal of Quantitative Spectroscopy and Radiative Transfer, J. Quant. Spectrosc. Ra., 153, 102-112, 2015.

Liu, J., Huang, J., and Chen, B.: Detecting dust aerosols in Sahara areas using CALIPSO lidar and IIR, the 28th annual meeting of China meteorological society, Xiamen, China, 2011.

Liu, Y., Huang, J., Shi, G., Takamura, T., Khatri, P., Bi, J., Shi, J., Wang, T., Wang, X., and Zhang, B.: Aerosol optical properties and radiative effect determined from sky-radiometer over Loess Plateau of Northwest China, Atmos. Chem. Phys., 11, 11455-11463, doi: 10.5194/acp-11-11455-2011, 2011.

Liu, Z., Liu, D., Huang, J., Vaughan, M., Uno, I., Sugimoto, N., Kittaka, C., Trepte, C., Wang, Z., Hostetler, C., and Winker, D.,: Airborne dust distributions over the Tibetan Plateau and surrounding areas derived from the first year of CALIPSO lidar observations, Atmos. Chem. Phys., 8, 5045-5060, doi:10.5194/acp-8-5045-2008, 2008b.

Liu, Z., Omar, A.., Hu, Y., Vaughan, M., and Winker, D.: CALIOP algorithm theoretical basis document, part 3: Scene classification algorithms, NASA-CNES document PC-SCI-203, 2005.

Luo, Y., Li, W., Zhou, X., He, Q., and Qing, J.: Analysis of the 1980's Atmospheric Aerosol Optical Depth over China, J. Meteor. Res., 59, 77-87, 2000.

Lüthi, Z., Škerlak, B., Kim, S., Lauer, A., Mues, A., and Rupakheti, M.: Atmospheric brown clouds reach the Tibetan Plateau by crossing the Himalayas, Atmos. Chem. Phys., 4, 28105-28146, doi: 10.5194/acp-15-6007-2015, 2014.

Platt, C., Lidar and Radiometric Observations of Cirrus Clouds, J. Atmos. Sci., 30, 1191- 1204, 1973.

Platt, C., Young, S., Manson, P., Patterson G., Marsden S., Austin, R., and Churnside, J., The optical properties of equatorial cirrus from observations in the arm pilot radiation observation experiment, J. Atmos. Sci., 1977-1996, 1998.

Sassen, K., Benson, S.: A midlatitude cirrus cloud climatology from the facility for atmospheric remote sensing. Part II: Microphysical properties derived from lidar depolarization, J. Atmos.

Sci., 58, 2103-2112, 2001.

Sassen, K.: Indirect climate forcing over the western US from Asian dust storms, Geophys. Res. Lett., 29(10), 1465, doi:10.1029/2001GL014051, 2002.

Shen, Z., Cao, J., Arimoto, R., Zhang, R., Jie, D., and Liu, S.: Chemical composition and source characterization of spring aerosol over Horqin sand land in northeastern China, J. Geophys. Res., 112, D14, doi: 10.1029/2006JD007991, 2007.

Shi, G., Wang, H., Wang, B., Li, W., Gong, S., and Zhao, T.: Sensitivity experiments on the effects of optical properties of dust aerosols on their radiative forcing under clear sky condition, J. Meteorol. Soc. Jpn., 83A, 333-346, doi:10.2151/jmsj.83A.333, 2005.

Sokolik, I., and Toon, O.: Direct radiative forcing by anthropogenic airborne mineral aerosols, Nature, 381, 681-683, doi:10.1038/381681a0, 1996.

Su, J., Huang, J., Fu, Q., Minnis, P., Ge, J., and Bi, J.: Estimation of Asian dust aerosol effect on cloud radiation forcing using Fu-Liou radiative model and CERES measurements, Atmos. Chem. Phys., 8, 2763-2771, doi:10.5194/acp-8-2763-2008, 2008.

Sugimoto, N., Nishizawa, T., Shimizu, A., Matsui, I., & Kobayashi, H.: Detection of internally mixed Asian dust with air pollution aerosols using a polarization optical particle counter and a polarization-sensitive two-wavelength lidar, J. Quant. Spectrosc. Ra, 150, 107-113, 2015b.

Sugimoto, N., Nishizawa, T., Shimizu, A., Matsui, I., Jin, Y., Higurashi, A., Uno, I., Hara, Y., Yumimoto, K., and Kudo, R.: Continuous observations of atmospheric aerosols across East Asia, Remote Sensing, doi: 10.1117/2.1201510.006178, 2015a.

Sun, Y., Zhuang, G., Wang, Y., Zhao, X., Li, J., Wang, Z., and An, Z.: Chemical composition of dust storms in Beijing and implications for the mixing of mineral aerosol with pollution aerosol on the pathway, J. Geophys. Res., 110, D24, doi:10.1029/2005JD006054, 2005.

Takemura, T., Uno, I., Nakajima, T., Higurashi, A., and Sano, I.: Modeling study of long-range transport of Asian dust and anthropogenic aerosols from East Asia, Geophys. Res. Lett., 29(24), doi/10.1029/2002GL016251, 2002.

Tegen, I. and Fung, I.: Contribution to the atmospheric mineral aerosol load from land surface modification, J. Geophys. Res., 100, 18707-18726, doi:10.1029/95JD02051, 1995.

Twomey, S., Piepgrass, M., and Wolfe, T.: An assessment of the impact of pollution on global cloud albedo, Tellus, Ser. B, 36, 356–366, 1984.

Wandinger, U., Tesche, M., Seifert, P., Ansmann, A., Muller, D., and Althausen, D.: Size matters: influence of multiple scattering on CALIPSO light-extinction profiling in desert dust, Geophys. Res. Lett., 37(10), L10801, 2010.

Wang, G., Huang, J., Guo, W., Zuo, J., Wang, J., Bi, J., Huang, Z., and Shi, J.: Observation analysis of land-atmosphere interactions over the Loess Plateau of northwest China, J. Geophys. Res., 115, D00K17, doi:10.1029/2009JD013372, 2010.

Winker, D. M., Vaughan, M. A., Omar, A., Hu, Y., Powell, K. A., Liu, Z., Hunt, W. and Young, S. A.: Overview of the CALIPSO mission and CALIOP data processing algorithms, J. Atmos. Ocean. Technol., 26(11), 2310-2323, 2009.

Xie, C., Nishizawa, T., Sugimoto, N., Matsui, I., and Wang, Z.: Characteristics of aerosol optical properties in pollution and Asian dust episodes over Beijing, China, Appl. Opt., 47(27), 4945-4951, 2008.

Young, S.: Analysis of lidar backscatter profiles in optically thin clouds, Appl. Opt., 34(30), 7019-7031, 1995.

Yu, H., Remer, L. A., Chin, M., Bian, H., Tan, Q., Yuan, T., and Zhang, Y.: Aerosols from overseas rival domestic emissions over North America, Science, 337, 566-569, doi:10.1126/science.1217576, 2012.

Zhang, R., Arimoto, R., An, J., Yabuki, S., and Sun, J.: Ground observations of a strong dust storm in Beijing in March 2002, J. Geophys. Res., 110, D18, doi: 10.1029/2004JD004589, 2005.

Zhou, T., Huang, J., Huang, Z., Liu, J., Wang, W., and Lin, L.: The depolarization-attenuated backscatter relationship for dust plumes, Opt. Express, 21(13), 15195-15204, 2013.

Zhou, T., Huang, Z., Huang, J., Li, J., Bi, J., and Zhang, W.: Study of vertical distribution of cloud over loess plateau based on a ground-based lidar system, J. Arid Meteor. (in Chinese), 31, 246-253, doi:10.11755/j.issn.1006-7639(2013)-02-0246, 2013.

**Figure captions:**

Figure 1. Spatial distribution of dust event in China, color represent the number of dust event, the locations of SACOL is shown in green pentagram, the nearby dust source (Taklimakan, Gobi) is also shown.

Figure 2. Structure of L2S-SM-II dual band depolarization lidar at SACOL (Zhou, et al, 2013).

Figure 3. Distribution of attenuated backscattering coefficient (a), linear volume depolarization ratio (b) and color ratio (c) measured by SACOL NIES on 31 March 2010.

Figure 4. Three-day back trajectories of air parcels passing by SACOL on 31 March 2010 by using NOAA HYSPLIT Model.

Figure 5. Distribution of attenuated backscattering coefficient (a), linear volume depolarization ratio (b) and color ratio (c) on 31 July 2010 by using SACOL NIES.

Figure 6. Six-day back trajectories of air parcels passing by the SACOL on 31 July 2010 by using NOAA HYSPLIT Model.

Figure 7. Comparison of the frequency distribution of linear volume depolarization ratio for pure dust (blue) and transported anthropogenic dust (red).

Figure 8. Comparison of the frequency distribution of color ratio for pure dust (blue) and transported anthropogenic dust (red).

Figure 9. Relationship between backscatter coefficient and linear volume depolarization ratio for (a) pure dust and (b) transported anthropogenic dust. The colors represent the percentage in each 0.02*0.0008 box and the value is scaled by 100.

Figure 10. Relationship between backscatter coefficient and color ratio for (a) pure dust and (b) transported anthropogenic dust. The colors represent the percentage in each 0.02*0.0008 box and the value is scaled by 100.

Atmos. Chem. Phys. Discuss., https://doi.org/10.5194/acp-2017-1000
Manuscript under review for journal Atmos. Chem. Phys.
Discussion started: 14 December 2017


Atmospheric Chemistry and Physics Discussions

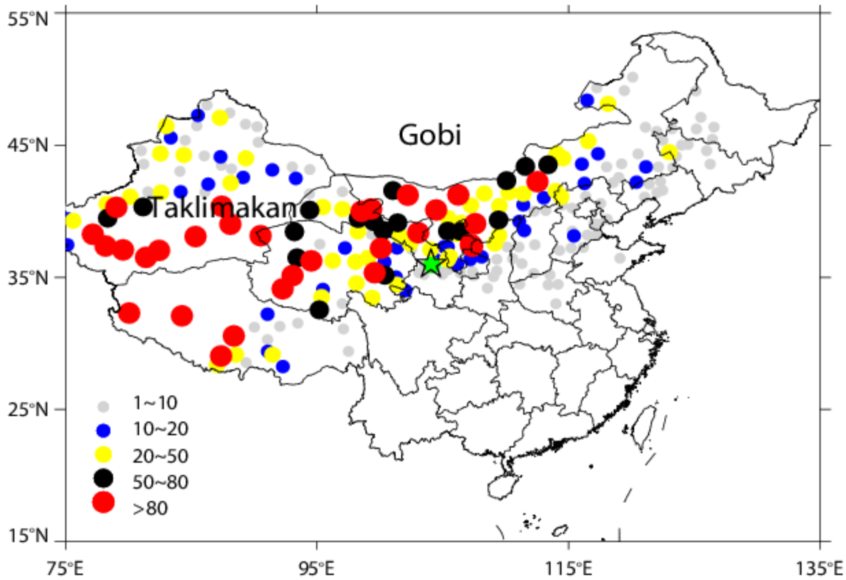


Figure 1. Spatial distribution of dust event in China, color represent the number of dust event, the locations of SACOL is shown in green pentagram, the nearby dust source (Taklimakan, Gobi) is also shown.

Atmos. Chem. Phys. Discuss., https://doi.org/10.5194/acp-2017-1000
Manuscript under review for journal Atmos. Chem. Phys.
Discussion started: 14 December 2017


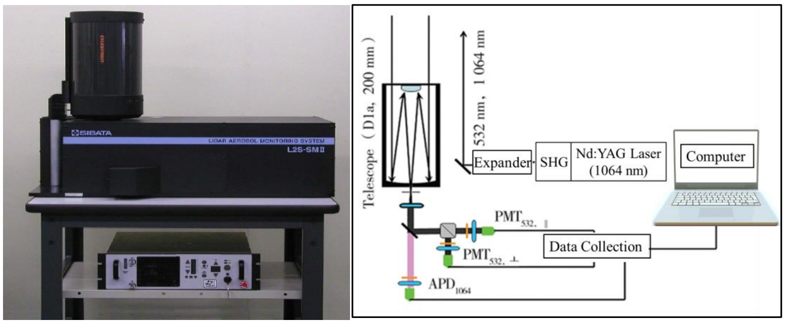


Figure 2. Structure of L2S-SM-II dual band depolarization lidar at SACOL (Zhou, et al, 2013).

Atmos. Chem. Phys. Discuss., https://doi.org/10.5194/acp-2017-1000
Manuscript under review for journal Atmos. Chem. Phys.
Discussion started: 14 December 2017


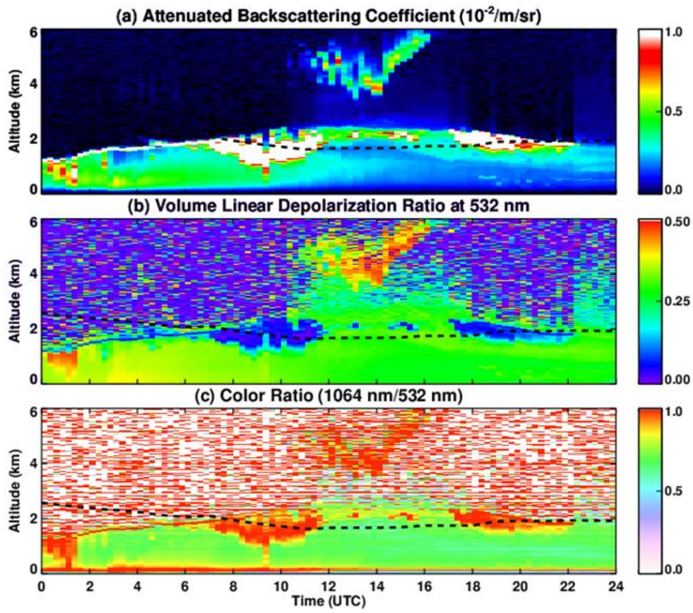


Figure 3. Distribution of attenuated backscattering coefficient at 532nm (a), linear volume depolarization ratio (b) and color ratio (c) measured by SACOL NIES on 31 March 2010. The black dotted line indicates NIES lidar PBL height via maximum standard deviation method (same as in the Huang et al., 2015).

Atmos. Chem. Phys. Discuss., https://doi.org/10.5194/acp-2017-1000
Manuscript under review for journal Atmos. Chem. Phys.
Discussion started: 14 December 2017


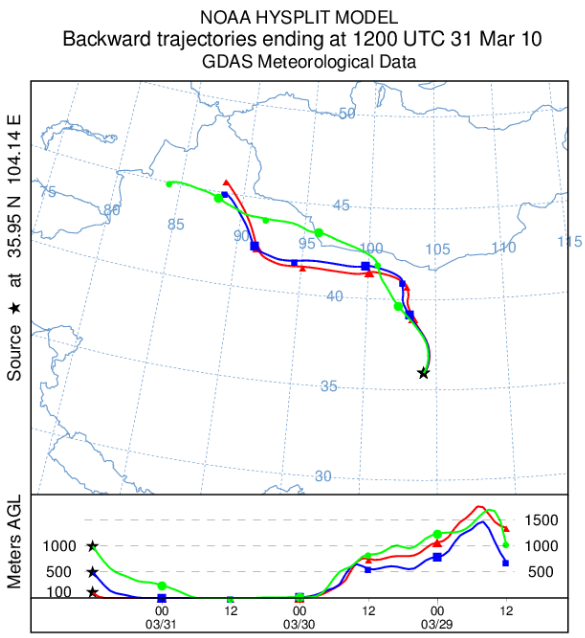


Figure 4. Three-day back trajectories of air parcels passing through SACOL on 31 March 2010 by using NOAA HYSPLIT Model.

Atmos. Chem. Phys. Discuss., https://doi.org/10.5194/acp-2017-1000
Manuscript under review for journal Atmos. Chem. Phys.
Discussion started: 14 December 2017


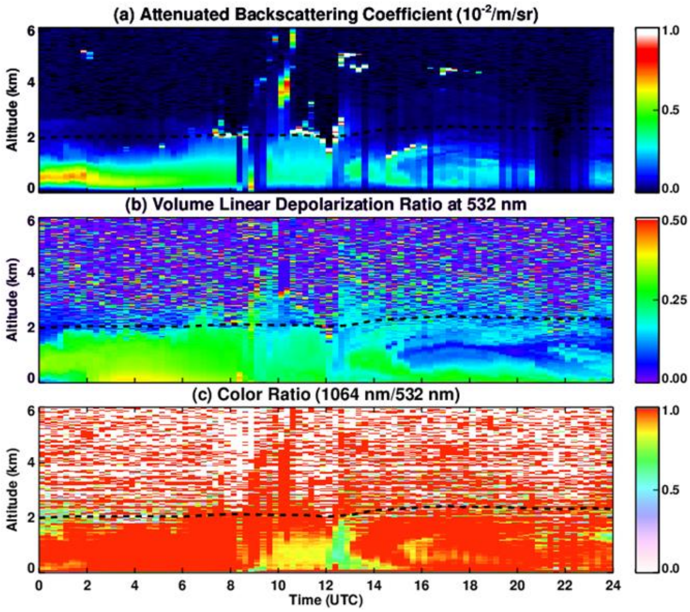


Figure 5. Distribution of attenuated backscattering coefficient at 532nm (a), linear volume depolarization ratio (b) and color ratio (c) on 31 July 2010 by using SACOL NIES. The black dotted line indicates NIES lidar PBL height via maximum standard deviation method.

Atmos. Chem. Phys. Discuss., https://doi.org/10.5194/acp-2017-1000
Manuscript under review for journal Atmos. Chem. Phys.
Discussion started: 14 December 2017


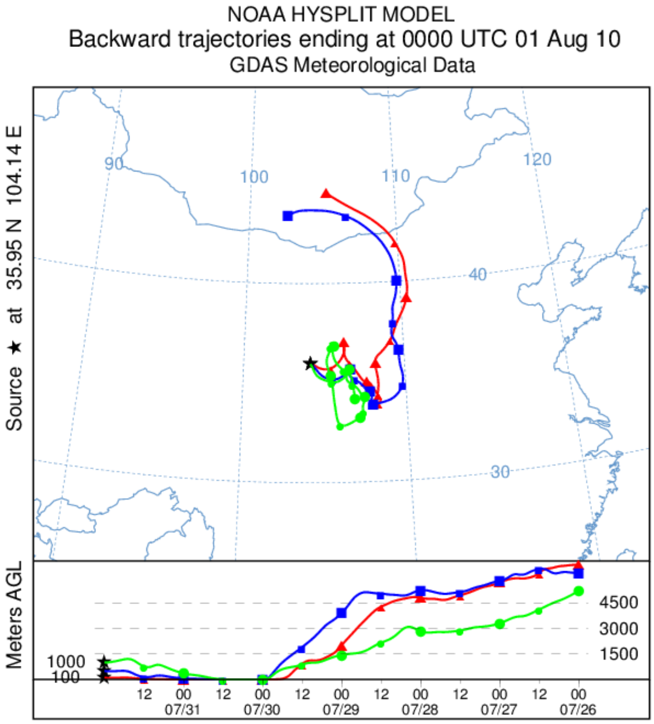


Figure 6. Six-day back trajectories of air parcels passing through the SACOL on 31 July 2010 by using NOAA HYSPLIT Model.

Atmos. Chem. Phys. Discuss., https://doi.org/10.5194/acp-2017-1000
Manuscript under review for journal Atmos. Chem. Phys.
Discussion started: 14 December 2017


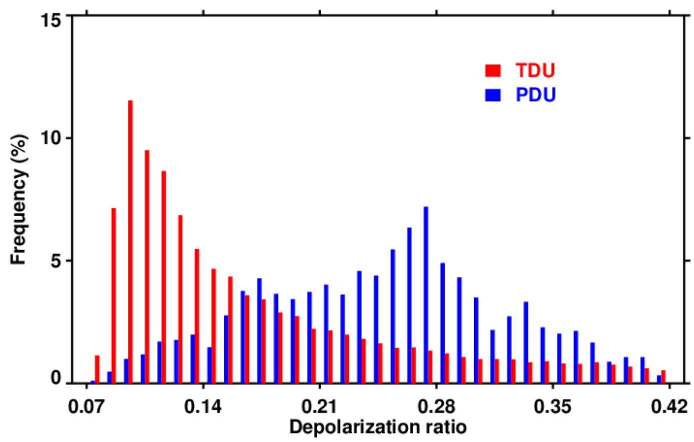


Figure 7. Comparison of the frequency distribution of linear volume depolarization ratio for pure dust (blue) and transported anthropogenic dust (red).

Atmos. Chem. Phys. Discuss., https://doi.org/10.5194/acp-2017-1000
Manuscript under review for journal Atmos. Chem. Phys.
Discussion started: 14 December 2017


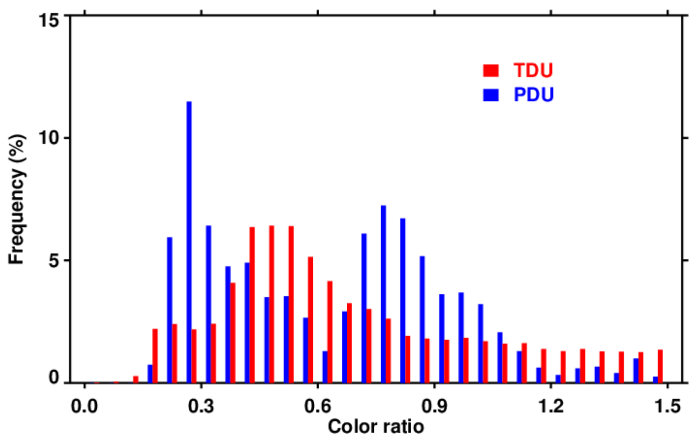


Figure 8. Comparison of the frequency distribution of color ratio for pure dust (blue) and transported anthropogenic dust (red).

Atmos. Chem. Phys. Discuss., https://doi.org/10.5194/acp-2017-1000
Manuscript under review for journal Atmos. Chem. Phys.
Discussion started: 14 December 2017


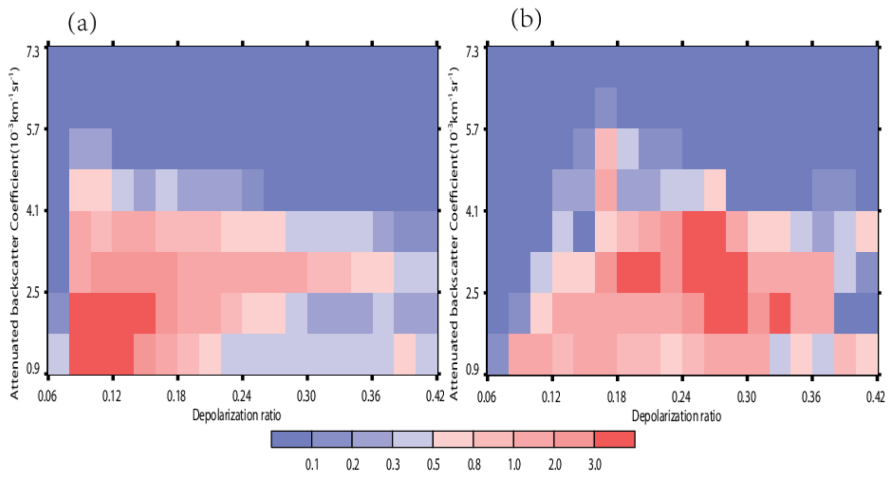


Figure 9. Relationship between backscatter coefficient and linear volume depolarization ratio for (a) pure dust and (b) transported anthropogenic dust. The colors represent the percentage in each 0.02*0.0008 box and the value is scaled by 100.

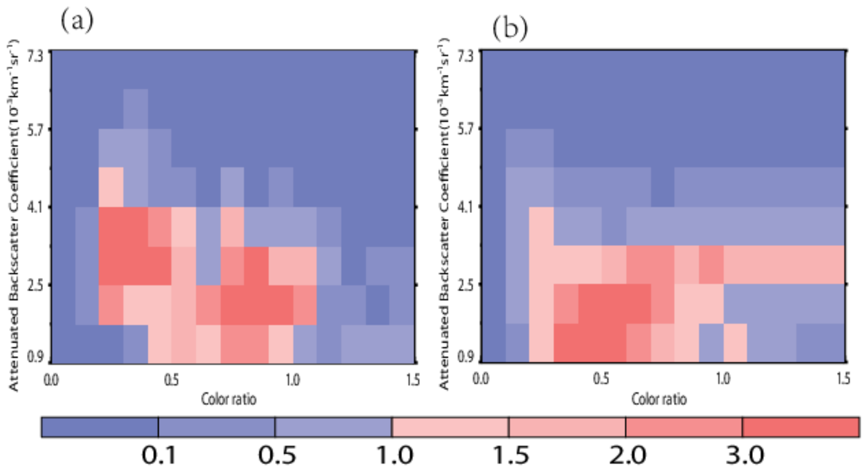


Figure 10. Relationship between backscatter coefficient and color ratio for (a) pure dust and (b) transported anthropogenic dust. The colors represent the percentage in each 0.02*0.0008 box and the value is scaled by 100.